

Electron tunneling through double-electric barriers on HgTe/CdTe heterostructure interface

Liang-Zhong Lin(林亮中), Yi-Yun Ling(凌艺纭), Dong Zhang(张东), and Zhen-Hua Wu(吴振华)
Citation: Chin. Phys. B, 2022, 31 (**11**): 117201. DOI: 10.1088/1674-1056/ac7a0f

What follows is a list of articles you may be interested in

Theoretical design of thermal spin molecular logic gates by using a combinational molecular junction

Yi Guo(郭逸), Peng Zhao(赵朋), and Gang Chen(陈刚)
Chin. Phys. B, 2022, 31 (**4**): 047202. DOI: 10.1088/1674-1056/ac3a5f

Understanding of impact of carbon doping on background carrier conduction in GaN

Zhenxing Liu(刘振兴), Liuan Li(李柳暗), Jinwei Zhang(张津玮), Qianshu Wu(吴千树), Yapeng Wang(王亚朋), Qiuling Qiu(丘秋凌), Zhisheng Wu(吴志盛), and Yang Liu(刘扬)
Chin. Phys. B, 2021, 30 (**10**): 107201. DOI: 10.1088/1674-1056/abfa0d

Group velocity matters for accurate prediction of phonon-limited carrier mobility

Qiao-Lin Yang(杨巧林), Hui-Xiong Deng(邓惠雄), Su-Huai Wei(魏苏淮), and Jun-Wei Luo(骆军委)
Chin. Phys. B, 2021, 30 (**8**): 087201. DOI: 10.1088/1674-1056/ac0133

Effect of weak disorder in multi-Weyl semimetals

Zhen Ning(宁震), Bo Fu(付博), Qinwei Shi(石勤伟), Xiaoping Wang(王晓平)
Chin. Phys. B, 2020, 29 (**7**): 077202. DOI: 10.1088/1674-1056/ab9612

Photoactive area modification in bulk heterojunctionorganic solar cells using optimization of electrochemicallysynthesized ZnO nanorods

Mehdi Ahmadi, Sajjad Rashidi Dafeh
Chin. Phys. B, 2015, 24 (**11**): 117203. DOI: 10.1088/1674-1056/24/11/117203

Electron tunneling through double-electric barriers on HgTe/CdTe heterostructure interface

Liang-Zhong Lin(林亮中)[1], Yi-Yun Ling(凌艺纭)[2], Dong Zhang(张东)[3], and Zhen-Hua Wu(吴振华)[4,†]

[1] *School of Information Engineering, Zhongshan Polytechnic, Zhongshan* 528400, *China*
[2] *School of Physics and Material Sciences, Guangzhou University, Guangzhou* 510000, *China*
[3] *SKLSM, Institute of Semiconductors, Chinese Academy of Sciences, Beijing* 100083, *China*
[4] *MEDIT, Institute of Microelectronics, Chinese Academy of Sciences, Beijing* 100029, *China*

(Received 10 February 2022; revised manuscript received 9 June 2022; accepted manuscript online 18 June 2022)

We investigate theoretically the carrier transport in a two-dimensional topological insulator of (001) HgTe/CdTe quantum-well heterostructure with inverted band, and find distinct switchable features of the transmission spectra in the topological edge states by designing the double-electric modulation potentials. The transmission spectra exhibit the significant Fabry–Pérot resonances for the double-electric transport system. Furthermore, the transmission properties show rich behaviors when the Fermi energy lies in the different locations in the energy spectrum and the double-electric barrier regions. The opacity and transparency of the double-modulated barrier regions can be controlled by tuning the modulated potentials, Fermi energy and the length of modulated regions. This electrical switching behavior can be realized by tuning the voltages applied on the metal gates. The Fabry–Pérot resonances leads to oscillations in the transmission which can be observed in experimentally. This electric modulated-mechanism provides us a realistic way to switch the transmission in edge states which can be constructed in low-power information processing devices.

Keywords: HgTe/CdTe quantum well, double-electric modulations, transmission spectra, Fabry–Pérot resonances

PACS: 72.10.–d, 73.40.–c, 73.40.Gk, 73.63.Hs **DOI:** 10.1088/1674-1056/ac7a0f

1. Introduction

Topological insulators (TIs) are a new class of materials that have been theoretically predicted[1–6] and demonstrated experimentally.[7–10] They are band insulators (BIs) in the bulk while conducting along the surfaces, possessing surface states with a spin texture protected by time-reversal symmetry. This kind of electron transport is robust against the nonmagnetic impurity scattering and local perturbation.[11–14] The concept of a topological insulator dates back to the work of Kane and Mele, who focused on two-dimensional (2D) systems.[1,2] The spin texture induced by spin–orbit interaction (SOI) in non-centrosymmetric materials has been regarded as a promising avenue for next-generation spintronics applications.[15–19] This offers great potential applications in a new generation of spintronic devices for low-power information processing.[20–24]

In 2D HgTe/CdTe quantum wells (QWs) with an inverted-band structure, the helical edge channels have been demonstrated experimentally in the Hall bar geometry.[7,8] There is plenty of research about the potential applications based on construct improved devices in HgTe and various TI material systems.[25–31] As a basic building block of the electric devices, the electric metal strip modulations have been studied extensively in various systems.[32–34] This offers great potential for a new generation of spintronic devices with low-power information processing. A crucial step in this development is the (preferentially electrical) manipulation, i.e., switch on or off, of the channel transport. Therefore, electrical manipulation of the transport property of TIs becomes one of the central issues in the condensed matter physics. It is highly desirable to achieve an electric control of the carrier transport related with this new class of materials.

In this work, we are particularly interested in HgTe/CdTe QWs because HgTe/CdTe is the first TI discovered in nature.[7,8] We investigate theoretically the carrier transport properties through the HgTe/CdTe QW heterostructure under double-electric modulations. The modulation potential can be controlled by the external voltages applied on the metal gate. As will be seen, rich transmission features will shown by changing the double-electric modulated parameters. Different transport processes can be achieved by tuning the modulations potential. The Fabry–Pérot resonances[32–35] can be observed due to the interference between double modulated regions. The transmission shows the Fabry–Pérot resonances for the inter-band tunneling process and is blocked for the intra-band process. The constructive interference of the backscattering by double modulations layers will lead to the block of transmission. Furthermore, the bulk gap of HgTe/CdTe QWs can be used to switch off the system. The transport property of the propagating states can also be controlled by the length of modulated regions.

†Corresponding author. E-mail: wuzhenhua@ime.ac.cn

© 2022 Chinese Physical Society and IOP Publishing Ltd

2. Model and formulations

We consider a HgTe/CdTe QW heterostructure with double-electric-modulation structures in planar geometry [as shown schematically in Fig. 1(a)]. A voltage gate is deposited on top of the heterostructure to create an electric modulation with bias V_g.[32,33] For simplicity, each electric potential is assumed to be of a step-like profile, i.e., $V = V_g$ in the modulated region and $V = 0$ otherwise. The electric modulation amplitude $e \cdot V_g$ can be tuned by adjusting the top gate voltage. The carriers injected from left lead can transmit or reflected under the double-electric modulated regions. An effective four-band model introduced by Bernevig, Hughes and Zhang (BHZ-model)[7,8] consists of two disconnected blocks (including two Γ_6 electron bands $|e\uparrow\rangle, |e\downarrow\rangle$ and two Γ_8 heavy hole bands $|hh\uparrow\rangle, |hh\downarrow\rangle$ by neglecting the light-hole and spin-split bands). The BHZ-model adequately describes the insulating regime in HgTe/CdTe QWs close to the Γ point and the topological quantum phase transition near the critical thickness $d = d_c$. The carriers states in the low-energy regime can be well described by a four-band effective Hamiltonian $\boldsymbol{H}_0$. In the presence of the double-electrical modulated potentials, the total 4×4 Hamiltonian in the basis $|e\uparrow\rangle, |hh\uparrow\rangle, |e\downarrow\rangle$, and $|hh\downarrow\rangle$ can be written as $\boldsymbol{H} = \boldsymbol{H}_0 + V_{g1} + V_{g2}$, with $\boldsymbol{H}_0$ given by[7]

$$\boldsymbol{H}_0 = \begin{pmatrix} \varepsilon_{\hat{\boldsymbol{k}}} + M(\hat{\boldsymbol{k}}) & A\hat{k}_- & 0 & 0 \\ A\hat{k}_+ & \varepsilon_{\hat{\boldsymbol{k}}} - M(\hat{\boldsymbol{k}}) & 0 & 0 \\ 0 & 0 & \varepsilon_{\hat{\boldsymbol{k}}} + M(\hat{\boldsymbol{k}}) & -A\hat{k}_+ \\ 0 & 0 & -A\hat{k}_- & \varepsilon_{\hat{\boldsymbol{k}}} - M(\hat{\boldsymbol{k}}) \end{pmatrix}, \quad (1)$$

where $\hat{\boldsymbol{k}} = (\hat{k}_x, \hat{k}_y)$ is the in-plane momentum operator, $\varepsilon_{\hat{\boldsymbol{k}}} = C - D(\hat{k}_x^2 + \hat{k}_y^2)$, $M(\hat{\boldsymbol{k}}) = M - B(\hat{k}_x^2 + \hat{k}_y^2)$, $\hat{k}_\pm = \hat{k}_x \pm \mathrm{i}\hat{k}_y$, and A, B, C, D, and M are parameters describing the band structure of the HgTe/CdTe QWs. The velocity operator $\hat{v}(x)$ along the x axis is given by

$$\hat{v}(x) = \begin{pmatrix} -2D_+\hat{k}_x & A & 0 & 0 \\ A & -2D_-\hat{k}_x & 0 & 0 \\ 0 & 0 & -2D_+\hat{k}_x & -A \\ 0 & 0 & -A & -2D_-\hat{k}_x \end{pmatrix}, \quad (2)$$

where $D_\pm = D \pm B$.

For a 2D system shown in Fig. 1(a), the total transmission and conductance are obtained by discretizing the system into j ($j = 5$) in this system as shown in Fig. 1(d)] transverse strips along the x axis. The interfaces coordinates are denoted by x_1, x_2, x_3, x_4 [see Fig. 1(e)]. The transverse wave vector k_y is conserved due to the homogeneous structure along the y direction. In a given strip j ($j = 1, \ldots, 5$), the eigenstates can be written as

$$\psi^j(x,y) = \chi^j \exp[\mathrm{i}(k_x^j x + k_y y)]. \quad (3)$$

The longitudinal wave vector $k_x = k_x^j$ is determined from the Schrödinger equation $E\psi = \boldsymbol{H}(k_x, k_y)\psi$. These eigenstates are classified into the right-moving states and left-moving states. The right-moving states have a real k_x and positive velocity $\langle\psi|\hat{v}_x|\psi\rangle$ or have a complex k_x with $\mathrm{Im}k_x > 0$. The left-moving states have a real k_x and negative velocity $\langle\psi|\hat{v}_x|\psi\rangle$ or have a complex k_x with $\mathrm{Im}k_x < 0$. For a given energy E, the mth right-moving state in the mth strip is denoted by $\psi_{m,+}^{(M)}(E)$ and the mth left-moving state is denoted by $\psi_{m,-}^{(M)}(E)$.

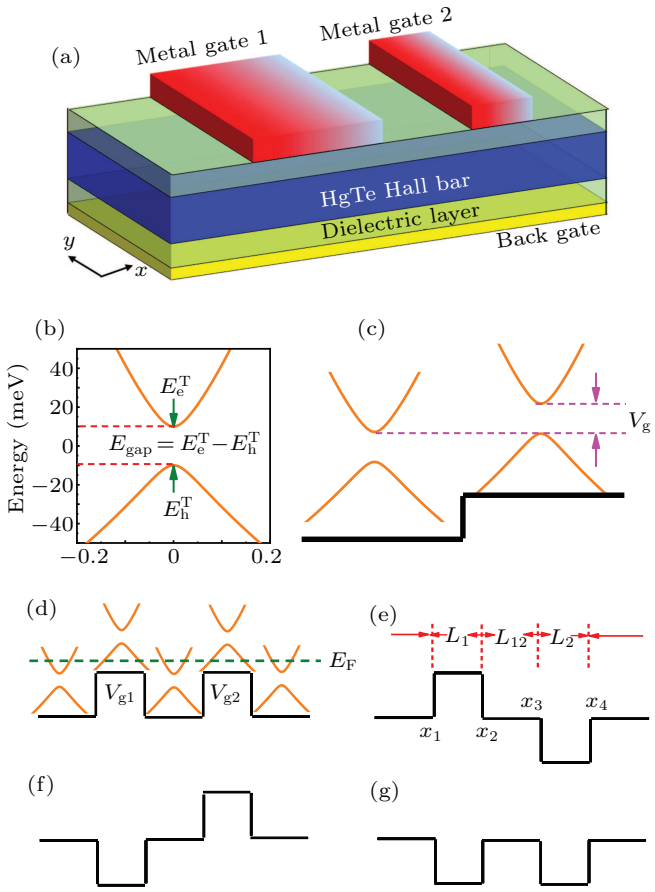


Fig. 1. (a) Schematic illustration of HgTe/CdTe QW heterostructure planar geometry with double gate-induced barriers created by two metallic strips on the surface. (b) The energy spectra for the considered HgTe/CdTe QW system. E_e^T is the lowest energy of the conduction-band (locates at the position $E = 10$ meV) and E_h^T is the highest energy of the valance-band (locates at the position $E = -10$ meV) of the energy dispersion. Thus, $E_{gap} = E_e^T - E_h^T = 20$ meV is the bulk gap of the system. (c) Schematic illustration of the E_{gap} shifted upwards V_g by the metal gate modulation potential. (d)–(g) Different configurations for the delta-function-shaped electric modulations. V_{g1} and V_{g2} indicate the electric modulation potential. L_1 and L_2 indicate the length of the first and second modulated region, respectively. L_{12} represents the length between double electric modulated regions. The energy dispersions in the different regions of the system shown in (d), and the horizontal dashed line indicates the Fermi energy E_F.

Assuming that one carrier with Fermi energy E_F is injected into the mth right-moving (with a real k_x) eigenstate $\psi_{m,+}^{(L)}$ of the left lead, the scattering wave function in left lead, jth transverse strip and right lead can be written as

$$\psi^{(\mathrm{Left})} = \psi_{m,+}^{(\mathrm{Left})}(E_F) + \sum_n b_n^{(\mathrm{Left})}(E_F)\psi_{n,-}^{(\mathrm{Left})}(E_F),$$

$$\psi^{(j)} = \sum_n a_n^{(j)}(E_F)\psi_{n,+}^{(j)}(E_F) + \sum_n b_n^{(j)}(E_F)\psi_{n,-}^{(j)}(E_F),$$

$$\psi^{(\mathrm{Right})} = \sum_n a_n^{(\mathrm{Right})}(E_\mathrm{F})\psi_{n,+}^{(\mathrm{Right})}(E_\mathrm{F}). \quad (4)$$

The transmission and reflection amplitudes ($t_{m,n}$ and $r_{m,n}$) can be obtained by matching the wave functions and the currents at the interface, which requires the continuity of wave functions and probability current density at each boundary,[36,37]

$$\begin{aligned}&\psi^{(j)}(x=x_\lambda,y)=\psi^{(j+1)}(x=x_\lambda,y),\\ &v(x_\lambda)\cdot\psi^{(j)}(x=x_\lambda,y)=v(x_\lambda)\cdot\psi^{(j+1)}(x=x_\lambda,y). \quad (5)\end{aligned}$$

Here x_λ ($\lambda=1,2,3,4$) indicate the interfaces coordinates and j ($=1,\ldots,5$) represent the transverse discretized strips (especially, when $j=1$ and 5 denote the left lead and right lead, respectively). By scattering matrix theory,[23] we obtain the total transmission probability from the Landauer–Büttiker formula[38,39]

$$\begin{aligned}T &= \sum_{m\in\mathrm{Left},n\in\mathrm{Right}} T_{n\leftarrow m}(E_\mathrm{F})\\ &= \sum_{m\in\mathrm{Left},n\in\mathrm{Right}} \frac{v_n^{\mathrm{Right}}}{v_m^{\mathrm{Left}}}\left|a_n^{\mathrm{Right}}(E_\mathrm{F})\right|^2, \quad (6)\end{aligned}$$

where the sum runs over all right-moving modes in the left and right leads.

3. Results and discussion

We first investigate the tunneling behavior of the electron through a planar double-electric modulations in the HgTe/CdTe QW system. We consider the parameters for the HgTe/CdTe QWs: $A=364.5$ meV·nm, $B=-686$ meV·nm^2, $C=0$, $D=-512$ meV·nm^2, and $M=-10$ meV. The TI ($M<0$) and BI ($M>0$) phases are distinguished by the different signs of the parameter M, which are determined by the thickness of the HgTe/CdTe QWs (the corresponding thickness is 7 nm).[7] To begin with, we present our numerical results for the total transmission probability T (V_{g1},V_{g2}) across the structure by tuning the double-electric modulation amplitude $V_{g1},V_{g2}=-100\sim100$ meV in Fig. 2. The interesting transport behavior on the interface can be perfectly transmitted, and the total backscattering has been studied before.[32,33] The electron in HgTe/CdTe QWs behaves as a photo that is injected from a material with a larger refractive index n_2 into a medium with a smaller refractive index n_1. The carriers will be completely reflected when the incident angle is larger than the critical angle θ_c. The critical angle θ_c can be determined by Snell's law, $\sin\theta_\mathrm{c}/\sin\theta_\mathrm{R}=k_\mathrm{F}^\mathrm{R}/k_\mathrm{F}^\mathrm{L}=n_\mathrm{R}/n_\mathrm{L}$, and thus $\theta_\mathrm{c}=\arcsin(k_\mathrm{F}^\mathrm{R}/k_\mathrm{F}^\mathrm{L})$, where k_F^R and k_F^L denote the wave vectors in the right and left leads, respectively. In order to investigate the transport properties in the double-electric-modulation system, the incidence angle should be fixed in $0<\theta_\mathrm{inject}<\theta_\mathrm{c}$, thus we fix the incidence angle $\theta_\mathrm{inject}=\pi/4$ in the investigation, which is smaller than the critical angle θ_c. Furthermore, we consider two situations for the location of the Fermi energy, i.e., conduction-band ($E_\mathrm{F}>10$ meV) and valance-band ($E_\mathrm{F}<-10$ meV) [as shown in Fig. 1(b)]. First, we set the Fermi energy in the $E_\mathrm{F}=15$ meV in Fig. 2, the inject energy located in the conduction-band and indicate that the incident particles are electrons. There are two transmission gaps Δ_gap^1 and Δ_gap^2 in the transmission spectrum in Fig. 2. The gaps Δ_gap^1 and Δ_gap^2 will block the transmission and can be used to switch off the transport system. Two main reasons are involved. On the one hand, the gap Δ_gap^m ($m=1,2$) arises from the bulk gap E_gap of the left lead shifted by the modulation potential V_{g1} and V_{g2} in the modulated regions, because of the absence of propagating states when Fermi energy E_F locates in the gap [as sketched in Fig. 1(c)]. On the other hand, they result from the photon-like behavior when the incident angle is not perpendicular to the interface and can be described by Snell's law. We can find the gap Δ_gap^n ($n=3,4$) induced by the same mechanism when the Fermi energy located in the valance-band as shown in Fig. 3. However, Δ_gap^n ($n=3,4$) are larger than Δ_gap^m ($m=1,2$), because of the different Fermi energies, i.e., different group velocities for the conduction and valence bands, resulting in different critical angles θ_c. The gaps Δ_gap^n ($n=3,4$) are more sensitive to the incident angle when the Fermi energy ($E_\mathrm{F}=-25$ meV) located in the valence band (as shown in Fig. 3).

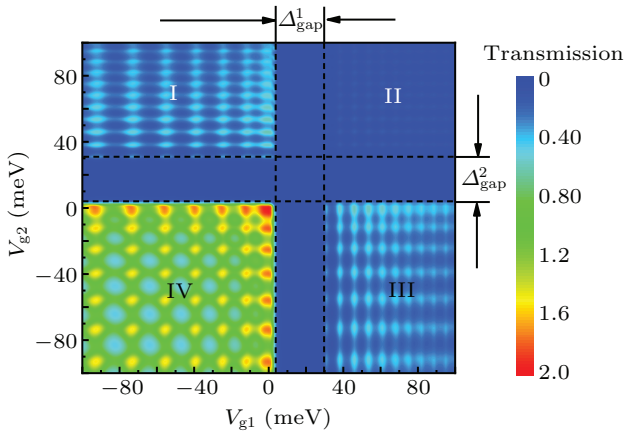


Fig. 2. Contour plot for the total transmission probability $T(V_{g1},V_{g2})$ of transmitted carrier as functions of double-electric modulations amplitude V_{g1} and V_{g2} for fixed Fermi energy $E_\mathrm{F}=15$ meV and incidence angle $\theta=\pi/4$. If not specified, $L_1=L_2=L_{12}=100$ nm.

By tuning the gate voltages, three tunneling processes can be realized: the intra-band process, the inter-band process, and the tunneling process through the modulations which are clearly reflected in Figs. 2 and 3. From the transmission spectra T (V_{g1},V_{g2}), we can divide it into four regions [marked by I, II, III, and IV in Fig. 2] by the two bulk gaps Δ_gap^1 and Δ_gap^2. By tuning the electric modulation potential V_{g1} and V_{g2}, different transport processes can be realized (see Fig. 2).

For $V_{g1}, V_{g2} \geq 25$ meV (inter-band process), the transmission probabilities approaching to the minimum $T(V_{g1}, V_{g2}) \approx 0$, i.e., the transmission is blocked, when the electrons transport through double-barriers structure [as shown in Fig. 1(d)]. The block originates from the multiple reflections in the electric modulated regions between multiple interfaces and gives rise to strong interference of backscattering. Therefore, when double-barrier amplitudes are large enough, they will block the transmission to result in the switch-off of the transport system [as shown in Fig. 2 marked by region Ⅱ]. When we set $V_{g1} \geq 30$ meV, $V_{g2} < 0$ [as shown in Fig. 2 marked by region Ⅲ] or $V_{g1} < 0$, $V_{g2} \geq 30$ meV [as shown in Fig. 2 marked by region I] (corresponding to inter-band and intra-band processes under double modulations), the transmission shown a slight regular oscillation around $T(V_{g1}, V_{g2}) = 0.1$–0.5, the decreasing oscillation amplitude resulting from the inter-band process by one of the modulation. When $V_{g1}, V_{g2} \leq 0$ [as shown in Fig. 2 marked by region Ⅳ] (corresponding to intra-band process), the Fabry–Pérot resonance tunneling processes are observed due to the quantum interference between the transmitted and reflected electrons across the double-electric modulated regions. Furthermore, when setting the Fermi energy $E_F = -25$ meV, the inject energy locates in the valance band and the incident particles are heavy holes in this system. The similar transmission processes (i.e., inter-band, intra-band and tunneling processes) can be found as we just discussed. The Fabry–Pérot resonances for Fermi energy $E_F = -25$ meV are more significant, the difference comes from group velocities for electrons and heavy holes are very different due to the different effective masses. More detailed features of the transmission spectra are shown in Fig. 3. Therefore, by tuning the double-modulation amplitude with gate voltages, the propagating states can be switched to different tunneling processes electrically when the carriers transmit through the structure.

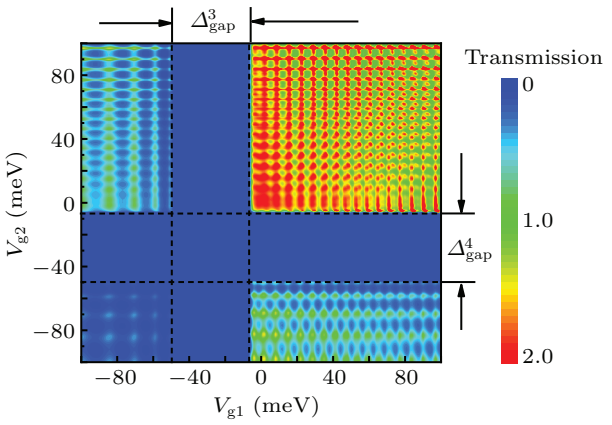


Fig. 3. Contour plot for the total transmission probability $T(V_{g1}, V_{g2})$ of transmitted carrier as functions of double-electric modulations amplitude V_{g1} and V_{g2} for fixed Fermi energy $E_F = -25$ meV and incidence angle $\theta = \pi/4$.

In order to see clearly the tunneling behavior under different-electric-modulation configurations, we show the total transmission $T(E_F)$ as a function of Fermi energy E_F for fixed incidence angle $\theta = \pi/4$ in Fig. 4. For double-barrier configuration [as shown in Fig. 1(d)], the Fabry–Pérot resonances are observed when the Fermi energy $E_F < -10$ meV [as clearly reflected by the blue solid line in Fig. 4(a)]. However, the transmission shows a slight oscillation for double-well configuration [as shown in Fig. 1(d)] as reflected by the orange dashed-dot line Fig. 4(a). The big gaps coming from the bulk gap E_{gap} shifted $|V_g|$ by the double electric modulations V_{g1} and V_{g2}, when the Fermi energy is located in the gap and is blocked, i.e., $T(E_F) = 0$. The gaps will become larger for the other two configurations [as shown in Figs. 1(e) and 1(f)] caused by the anti-parallel modulations configurations, the bulk gap will shifted by $|V_{g1}| + |V_{g2}|$ by the double electric modulations potential, resulted from the two main reasons that we have just explained it in the above section. The gaps will block the transmission and this coincides with the transmission spectra as shown in Fig. 4(b). Furthermore, the transmission spectra $T(E_F)$ seem to behave the same for the two-anti-parallel-modulation configuration [as confirmed by the coincidence of solid and dashed lines in Fig. 4(b)].

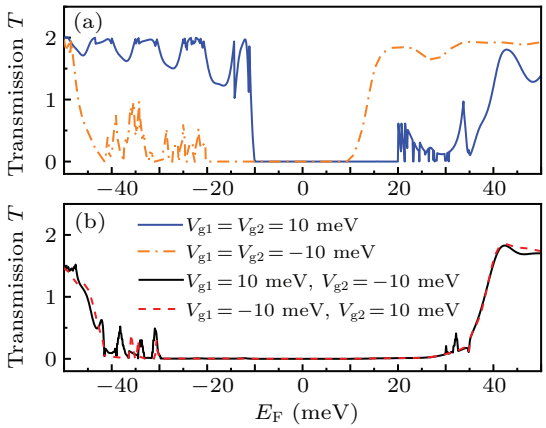


Fig. 4. The total transmission probability T as a function of Fermi energy E_F (for fixed gate voltage V_{g1} and V_{g2} and incidence angle $\theta = \pi/4$) for different-electric-modulation configurations [as indicated by different color lines (a) and (b)]. The blue solid, orange dashed-dot, black solid, and red dashed lines correspond to the configurations in Figs. 1(d)–1(g), respectively.

In Fig. 5, we show the total transmission $T(L_{12})$ variations with the distance between two applied biases for fixed Fermi energy and the electric potential. The Fermi energy $E_F = -15$ meV locates in the valance band, the transmission is oscillating regularly with the distance L_{12} for fixed $V_{g1} = V_{g2} = 10$ meV [as shown by black solid line in Fig. 5(a)]. The oscillation originates from the Fabry–Pérot interference between the transmitted and reflected carriers in the electric modulated regions. The same oscillation of transmission can be found when Fermi energy $E_F = 15$ meV locates in the conduction-band for modulations potential $V_{g1} = V_{g2} = -10$ meV [as shown by orange dashed line in Fig. 5(a)]. The oscillation arises from

the same mechanism, e.g., the Fabry–Pérot resonances tunneling process. Furthermore, the transmission shows a slight oscillation around $T\,(L_{12}) = 0.07$–0.12 for the anti-parallel-modulation configurations [corresponding to Figs. 1(e) and 1(f)] as clearly reflected in Fig. 5(b). The electric barrier in the anti-parallel-modulation configurations leading to the constructive interference of backscattering from double modulations layers, resulting in the decreasing transmission amplitude. We can expect that the transmission spectra in the configurations of two different anti-parallel modulations will complete coincidence with each other, this is confirmed in Fig. 5(b).

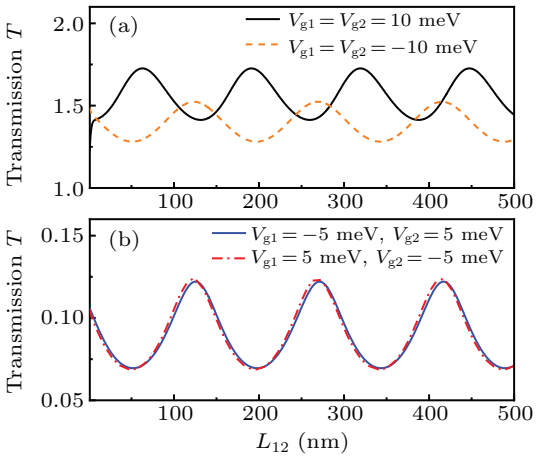


Fig. 5. The total transmission probability T as a function of the length between double electric modulated regions L_{12} with fixed incidence angle $\theta = \pi/4$ and electric modulations potential. (a) The black solid and orange dashed lines corresponding to $E_F = -15$ meV, $V_{g1} = V_{g2} = 10$ meV and $E_F = 15$ meV, $V_{g1} = V_{g2} = -10$ meV, respectively. (b) For a given Fermi energy $E_F = 15$ meV, located in the conduction band. The blue solid and red dashed-dot lines correspond to $V_{g1} = -5$ meV, $V_{g2} = 5$ meV and $V_{g1} = 5$ meV, $V_{g2} = -5$ meV, respectively.

Now we investigate the total transmission probability $T\left(L_{\text{length}}\right)$ as functions of the length of the double-electric modulated regions L_1 and L_2 for setting incidence angle and Fermi energy (see Fig. 6). The lengths of double modulated regions are changed simultaneously ($L_{\text{length}} = L_1 = L_2$). First, we set Fermi energy $E_F = 25$ meV located in the conduction band and plot in Fig. 6(a) the transmission probability $T\left(L_{\text{length}}\right)$ across the double-barrier modulation structure. For slight electric modulation amplitude $V_{g1} = V_{g2} = 5$ meV, the transmission $T\left(L_{\text{length}}\right)$ oscillating periodically with the increasing length L_{length} [as sketched by black line in Fig. 6(a)]. The regular oscillation also originates from the Fabry–Pérot interference since the velocities of propagating bulk states in different regions are different due to the potential of modulations. In this case, electrons can propagate through the electric modulated regions. However, the transmission decreases with increasing L_{length} and finally becomes blocked for large electric modulation amplitude $V_{g1} = V_{g2} = 10$ meV [as clearly reflected by red dashed line in Fig. 6(a)]. The decreasing arises from the constructive quantum interference of backscattering amplitudes by different modulation layers. Therefore, the transmission decays exponentially with the barriers length L_{length}. For Fermi energy $E_F = -25$ meV located in the valance band, we can find the same periodic oscillation and decay behaviors of the transmission for different electric modulations potential [as shown in Fig. 6(b)]. The slight difference of the transmission spectra comes from the different effective masses between electron and heavy hole, which is decided by the incident Fermi energy.

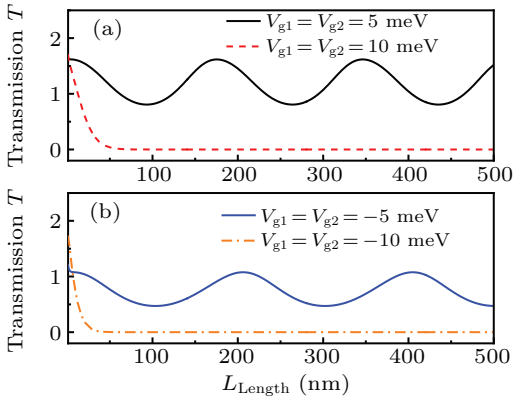


Fig. 6. The total transmission probability T as functions of the length of the double-electric modulated regions L_{length} ($L_{\text{length}} = L_1 = L_2$) with fixed incidence angle $\theta = \pi/4$ for different Fermi energies: (a) $E_F = 25$ meV, (b) $E_F = -25$ meV.

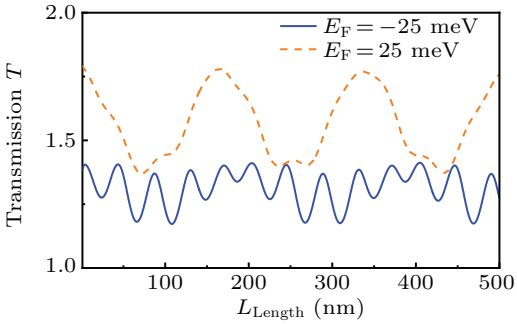


Fig. 7. The total transmission probability T as the length of the double-electric modulated regions L_{length} ($L_{\text{length}} = L_1 = L_2$) for fixed gate voltage $V_{g1} = -5$ meV and $V_{g2} = 5$ meV and incidence angle $\theta = \pi/4$. The blue solid and orange dashed lines correspond to $E_F = -25$ meV and $E_F = 25$ meV, respectively.

Finally we study the transmission $T\left(L_{\text{length}}\right)$ as functions of the length of the double-electric modulated regions L_1 and L_2 for one of the anti-parallel modulation configuration structure [as schematic illustrated in Fig. 1(f)]. The transmission oscillate periodically with the increasing length L_{length} for fixed incidence angle and Fermi energy (as shown in Fig. 7). The anti-parallel modulation configuration induces a series of resonances in the transmission spectrum (as shown in Fig. 7. These resonant peaks come from Fabry–Pérot resonances in the electric modulated regions at a proper incident angle for a fixed Fermi wave vector. The interference between the transmitted and reflected electrons leads to a series of Fano resonances in the transmissions spectrum. For the other anti-parallel modulation configuration structure [as schematic illustrated in Fig. 1(e)], we can expect the same transmission

spectra for the two anti-parallel modulation configurations as we discussed in the above subsection.

4. Conclusions

In summary, we have investigated theoretically the transport properties of carriers through inverted-band HgTe/CdTe QW topological interface states by double-electric barrier modulations, and found distinct switchable features of the transmission spectra by adjusting the double-electric modulation potentials. The opacity and transparency of the double-modulated regions can be controlled by tuning the modulated potentials, Fermi energy and the length of modulated regions. The Fabry–Pérot resonances lead to a series of oscillation in the transmission which can be observed experimentally. This electrical switching behavior can be manipulated by tuning the voltages applied on the metal gates. It may pave a way to manipulate the transmission to constructing low-power information processing devices by all electrical way.

Acknowledgements

Project supported by the College Innovation Project of Guangdong Province (Grant No. 2020KTSCX329), the Social Public Welfare and Basic Research Project of Zhongshan City (Grant No. 2020B2044), Zhongshan Polytechnic High-level Talents Project (Grant No. KYG2102), the National Key R&D Program of China (Grant No. 2021YFA1200502), and the National Natural Science Foundation of China (Grant No. 12174423).

References

[1] Kane C L and Mele E J 2005 *Phys. Rev. Lett.* **95** 226801
[2] Kane C L and Mele E J 2005 *Phys. Rev. Lett.* **95** 146802
[3] Fu L and Kane C L 2007 *Phys. Rev. B* **76** 045302
[4] Sheng D N, Weng Z Y, Sheng L and Haldane F D M 2006 *Phys. Rev. Lett.* **97** 036808
[5] Fu L, Kane C L and Mele E J 2007 *Phys. Rev. Lett.* **98** 106803
[6] Qi X L and Zhang S C 2011 *Rev. Mod. Phys.* **83** 1057
[7] Bernevig B A, Hughes T L and Zhang S C 2006 *Science* **314** 1757
[8] König M, Wiedmann S, Brüne C, Roth A, Buhmann H, Molenkamp L W, Qi X L and Zhang S C 2007 *Science* **318** 766
[9] Roth A, Brne C, Buhmann H, Molenkamp L W, Maciejko J, Qi X L and Zhang S C 2009 *Science* **325** 294
[10] Knez I, Du R R and Sullivan G 2011 *Phys. Rev. Lett.* **107** 136603
[11] Wu Z and Peeters F M and Chang K 2010 *Phys. Rev. B* **82** 115211
[12] Wu Z, Peeters F M and Chang K 2011 *Appl. Phys. Lett.* **98** 162101
[13] Lin L, Cheng F, Zhang L B, Zhang D and Yang W 2013 *Phys. Rev. B* **87** 245311
[14] Anversa J, Piquini P, Fazzio A and Schmidt T M 2014 *Phys. Rev. B* **90** 195311
[15] Wu Z and Li J 2012 *Nanoscale Res. Lett.* **7** 90
[16] Li J, Yang W, Liu J T, Huang W, Li C and Chen S Y 2017 *Phys. Rev. B* **95** 035308
[17] Li J and Chang K 2009 *Appl. Phys. Lett.* **95** 222110
[18] Gospodaric J, Dziom V, Shuvaev A, Dobretsova A A, Mikhailov N N, Kvon Z D and Pimenov A 2019 *Phys. Rev. B* **99** 115130
[19] Peter A J and Chang W L 2012 *Chin. Phys. Lett.* **29** 117201
[20] Gu X R, Guo L D and Sun X N 2018 *Chin. Phys. B* **27** 107202
[21] Peng X K and Zhang Z Z 2019 *Chin. Phys. B* **28** 127202
[22] Wu Z, Lin L, Yang W, Zhang D, Shen C, Lou W, Yin H and Chang K 2017 *RSC Adv.* **7** 30963
[23] Wu Z, Luo K, Yu J and Lin L 2018 *Solid State Commun.* **270** 151
[24] Lin L, Liu Y, Yu J, Zhu J, Zhang D and Wu Z 2021 *Physica E* **125** 114427
[25] Zhu J J, Yao D X, Zhang S C and Chang K 2011 *Phys. Rev. Lett.* **106** 097201
[26] Chang K and Lou W K 2011 *Phys. Rev. Lett.* **106** 206802
[27] Krueckl V and Richter K 2011 *Phys. Rev. Lett.* **107** 086803
[28] Hao R R, Zang R X, Zhou T, Kang S S, Yan S S, Liu G L, Han G B, Yu S Y and Mei L M 2019 *Chin. Phys. B* **28** 037202
[29] Wang Z C 2018 *Chin. Phys. B* **27** 016701
[30] Guo F, Wu Y P, Wu Z M, Chen T, Li H, Zhang C M, Fu M M, Lu Y H and Kang J Y 2018 *Chin. Phys. B* **27** 017502
[31] Lou W, Yang W and Chang K 2022 *Phys. Rev. B* **105** 045305
[32] Zhang L B, Zhai F and Chang K 2010 *Phys. Rev. B* **81** 235323
[33] Zhang L B, Chang K, Xie X C, Buhmann H and Molenkamp L W 2010 *New J. Phys.* **12** 083058
[34] Zhang L B, Cheng F, Zhai F and Chang K 2011 *Phys. Rev. B* **83** 081402(R)
[35] Li X, Wu Z and Liu J 2017 *Scientific Reports* **7** 6526
[36] Griffith S 1953 *Trans. Faraday Soc.* **49** 345
[37] Griffith S 1953 *Trans. Faraday Soc.* **49** 650
[38] Büttiker M, Imry Y, Landauer R and Pinhas S 1985 *Phys. Rev. B* **31** 6207
[39] Landauer R 1970 *Philos. Mag.* **21** 863